Bioelectrochemistry 165 (2025) 108941

Contents lists available at ScienceDirect

Bioelectrochemistry

journal homepage: www.journals.elsevier.com/bioelectrochemistry

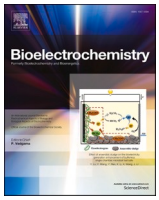

Modelling enzyme electrodes – What do we learn and how is it useful?

Philip N. Bartlett *, M. Hashim Khan

School of Chemistry and Chemical Engineering, University of Southampton, Southampton SO17 1BJ, UK

ARTICLE INFO

Keywords:
Modelling
Enzyme electrode
Redox-hydrogel
Case diagram

ABSTRACT

There has been an enormous increase in the computational power readily available since the first numerical treatments of electrochemical problems in the early 1960s. This development has been accompanied by the development of powerful, widely available, commercial software modelling tools. Despite this, approximate analytical treatments remain extremely useful in the modelling of coupled diffusion/reaction problems in electrochemistry because of the insights they provide into the different possible behaviours of the system. In this paper we discuss the modelling of amperometric enzyme electrodes, taking as our exemplar redox hydrogel-based enzyme electrodes in which the enzyme is immobilized in a redox active polymer which wires the enzyme to the electrode. In this system the measured current is related to many different experimental variables including substrate concentration and diffusion coefficient, reaction rate constants, and film properties and thickness. The interplay of these factors is described and the role of Case diagrams in understanding coupled diffusion/reaction problems of this type is discussed.

1. Introduction

In an amperometric enzyme electrode the current is related, in some complex way, to many different experimental variables. Some of these experimental variables, such as the concentration of the enzyme substrate or the electrode potential, are easily varied. Some of the variables, such as the enzyme loading, mediator concentration, enzyme kinetics or the diffusion coefficients of the different species, are more difficult to alter. In principle, changing one or more of these experimental variables can affect the response of the electrode and separating out these effects is challenging. Typically, experimentally one has access to a calibration curve, that is a plot of enzyme electrode current as a function of substrate concentration, and would like to optimize this for a particular application. However, to do this it is necessary to understand how the enzyme electrode functions and the factors that need to be addressed in order to improve the performance to meet practical requirements such as limit of detection, sensitivity, or long-term stability. Similar considerations apply in other electrochemical applications such as biofuel cells or photoelectrochemical energy conversion.

Modelling offers a way to gain insight into the operation of enzyme electrodes and to allow rational design for practical applications. In this paper we will discuss the different approaches to modelling of amperometric enzyme electrodes, including digital simulation tools and approximate analytical approaches. We will highlight the strengths and advantages of each approach and discuss the application of these to the analysis of experimental data taking as a particular example electrodes in which the enzyme is immobilized in a redox-hydrogel layer at the electrode surface which wires [1] the enzyme to the electrode.

2. Simulation and modelling

The topic of digital simulation in electrochemistry traces its history back to the pioneering work of Feldberg and Auerbach in 1964 [2]. They used an IBM 7094 digital computer programmed in the Fortran language to analyse current reversal chronopotentiograms for the EC mechanism with second order kinetics, that is an electrode reaction followed by a second order chemical reaction in solution. For this problem the second order kinetics renders the differential equations describing the combined diffusion/reaction problem unsolvable. The Fortran program (63 lines of code) took 11 min to run on a state-of-the-art, for that period, IBM 7094 which was a second-generation solid state mainframe computer (the particular IBM model had been introduced in 1962 and cost at that time ca. $3 m). Their simulation was a 1D simulation that used the simple “box method” in which the distance into solution from the electrode surface was divided into a number of boxes of equal size.

A significant step forward was taken by Joslin and Pletcher in 1974 [3] with the introduction of an expanding space grid in which the boxes are smaller close to the electrode surface, where concentration profiles

* Corresponding author.
E-mail address: P.N.Bartlett@soton.ac.uk (P.N. Bartlett).

https://doi.org/10.1016/j.bioelechem.2025.108941
Received 29 November 2024; Received in revised form 4 February 2025; Accepted 10 February 2025
Available online 22 February 2025

are changing more rapidly, and larger further from the electrode surface. This significantly improves the computational efficiency for many electrochemistry problems. An excellent introduction to digital simulation can be found in Britz's book "Digital Simulation in Electrochemistry" first published in 1981 [4] and now in its fourth edition [5].

In the early 1980s there was considerable interest in the topic of modified electrodes, and in particular in their application in redox catalysis. This led to the development of approximate analytical models by Andrieux, Dumas-Bouchiat and Savéant [6] and independently by Albery and Hillman [7] to describe the coupled mass transport and reaction of species within redox polymer films at electrode surfaces. In this case there is an irreversible second order homogeneous chemical reaction between the immobilized catalytic redox centre, $\sim M_{ox/red}$, and the reactant, S, diffusing into the polymer layer

$$\sim M_{ox} + S \xrightarrow{k_2} \sim M_{red} + P \quad (1)$$

described by a second order homogeneous rate constant k_2. This second order chemical reaction is coupled to diffusion of reactant into the film and charge propagation by redox hopping between $\sim M_{ox}$ and $\sim M_{red}$ through the polymer. Thus, these models are the progenitors of the later models for amperometric enzyme electrodes in which the second order chemical reaction is replaced by reactions of the enzyme immobilized within the layer at the electrode surface.

With the development of amperometric enzyme electrodes, starting from the first glucose biosensors, numerical models and approximate analytical models for amperometric enzyme electrodes were developed with a variety of approximate analytical treatments based on different simplifying assumptions including linearisation of the reaction kinetics or treatments for thin films where concentration polarisation of substrate within the film can be neglected. Examples can be found in the work of Calvo et al. [8], Tatsuma and Watanabe [9], Marchesiello and Genies [10], and Bourdillon et al. [11] from the early 1990s. A detailed review of modelling of amperometric enzyme electrodes up to 2005 can be found in the literature [12].

Over the period from 1964 to the present day the amount of computing power readily available to the electrochemist has increased enormously and with this increase powerful software tools such as DigiElch®, MATLAB® [14], Mathematica®, and COMSOL Multiphysics® [15] have become available to simulate a wide variety of complex electrochemical systems. Thus, the question arises, if we have much more powerful simulation tools why do we still need approximate analytical models? The problem with purely numerical simulations is that they don't provide insight and understanding of the steps that are rate limiting, or of the location of the reaction(s), and they don't allow you to simply optimize the electrode for a particular application. The most powerful approach is to combine the approximate analytical solutions with the numerical modelling, making use of the different strengths of the two approaches to get the best of both worlds.

3. Redox hydrogel-based enzyme electrodes

To illustrate our approach to modelling we will use amperometric enzyme electrodes in which the enzyme is immobilized in a redox-hydrogel at the electrode surface as our exemplar. This is a very popular and successful way to couple redox enzymes to electrodes, first introduced by Heller, in which the redox-hydrogel provides an immobilized mediator to shuttle charge from the active site of the redox enzyme to the electrode [16,17]. The same general approach to modelling can be applied to other types of biosensor, potentiometric, conductometric, etc., and to other problems, such as photogalvanic cells [18,19], and diffusion and binding in polymer films [20].

In the redox-hydrogel the mediator species, typically an osmium complex, Fig. 1a, is attached to the crosslinked water-soluble polymer chain by a flexible linker and the enzyme is physically entrapped within the layer. Because the mediator is complexed to the polymer chain in both redox states it cannot leach out of the film. Charge transport through the hydrogel occurs by self-exchange reactions between the redox sites and can be described by an apparent diffusion coefficient, D_{app}, (the Dahms-Ruff model [21–24]) where.

$$D_{app} = D + k\delta[M]\theta \quad (2)$$

Here D describes physical diffusion (so in this case D is zero since the redox groups are fixed), k is the self-exchange rate constant, δ is the distance for electron transfer, [M] is the mediator concentration and θ is a geometric factor (1/6 for 3-dimensional charge hopping). For a more detailed discussion, including the effects of percolation, see Blauch and Savéant [25]. D_{app} is predominantly determined by the segmental mobility, which increases with hydration and decreases upon excessive cross-linking. Typical values for D_{app} for Os redox hydrogels are around 10^{-8} cm^2 s^{-1} [17,26].

These redox-hydrogels have four important properties [16]: first they swell significantly in water so that they are an electron-conducting aqueous phase, second they can connect electrically multilayers of enzyme molecules to the electrode, third the orientation of the enzyme does not matter, and fourth they are highly permeable so molecules can diffuse in to and out of the film from the bulk solution. The properties of the redox-hydrogels can be tuned in terms of their permeability,

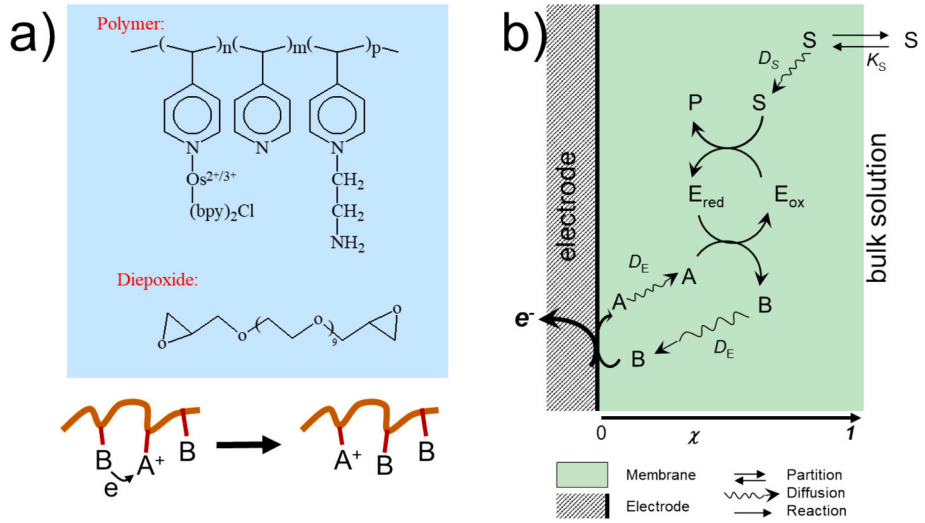

Fig. 1. a) Components of osmium redox hydrogel film. b) Reaction and transport steps in redox hydrogel enzyme electrode.

swelling and the apparent charge diffusion coefficient by changing the degree of crosslinking, the length of the linker to the osmium complex, and the nature of the substituents on the polymer chains. The redox potential of the Os redox couple can be adjusted by changing the complexation of the osmium. As a result, osmium redox-hydrogels have found wide application in enzyme electrodes and biofuel cells.

4. Setting up the problem

The set of reactions occurring in the redox-hydrogel on the working enzyme electrode is shown schematically in Fig. 1b. The reaction of the substrate, S, with the enzyme, E_{ox}, is described by Michaelis Menten kinetics

$$S + E_{ox} \overset{K_M}{\leftrightarrow} ES \overset{k_{cat}}{\rightarrow} P + E_{red} \tag{3}$$

where K_M is the Michaelis constant and k_{cat} is the turnover frequency. The reaction between the mediator and the enzyme is described by the second order rate constant k_A

$$E_{red} + \zeta A \overset{k_A}{\rightarrow} E_{ox} + \zeta B \tag{4}$$

where ζ is the stoichiometric factor. The reduced mediator is then reoxidised at the electrode surface

$$B \overset{k_{het}}{\rightarrow} A + ne \tag{5}$$

For the case of an osmium redox couple and glucose oxidase (GOx) this is a simplification because the enzyme is a homodimer with two separate flavin active sites [27]. However, there is no evidence of communication between the two flavin active sites within the homodimer. Further, the reaction of the oxidised flavin (FAD) with glucose oxidase to give the reduced $FADH_2$ is a two-electron reaction whereas the reverse reaction with the one electron osmium redox couple must happen in two steps and proceed through a semiflavin (FADH•) intermediate species.

$$GOx(FADH_2) + Os(III) \rightarrow GOx(FADH^{\bullet}) + Os(II) + H^+ \tag{6}$$

$$GOx(FADH^{\bullet}) + Os(III) \rightarrow GOx(FAD) + Os(II) + H^+ \tag{7}$$

(It is actually more complex than this because of the different protonation equilibria of the flavin, see Bourdillon et al. [28]). Consequently, k_A is the apparent rate constant describing the reoxidation of the reduced GOx by osmium(III). A further complication is that the GOx is specific for the oxidation of β-D-glucose which is one of the different isomers of D-glucose that exists in equilibrium in aqueous solution [27] and this should be taken into account when comparing experimental data to the results of modelling [29].

In an actual amperometric enzyme electrode, or in a biofuel cell, we have diffusion (for the substrate, both in solution and in the hydrogel and for charge propagation in the hydrogel as described by Dahms-Ruff), enzyme/substrate kinetics, and enzyme/mediator kinetics coupled together within the film. To understand the experimental results and how the current relates to these processes and which processes are rate limiting we need to develop a model. The reason why there are so many different models and simplifications is because the problem is difficult. Why is this difficult? It is difficult because there are different kinetic steps coupled together in the same spatial region and because the kinetics are non-linear. As a consequence there is no analytical solution to the problem, and we are forced to look for simplifications that make parts of the problem tractable and to use approximate analytical approaches and/or numerical simulation.

5. Deriving the approximate analytical solutions

In 1-dimension, corresponding to planar diffusion at a macroelectrode, the set of equations we have to solve is (assuming for simplicity that $\zeta = 1$)

$$\frac{\partial [A](x,t)}{\partial t} = D_A \frac{\partial^2 [A](x,t)}{\partial x^2} - k_A [E_{red}][A] \tag{8}$$

$$\frac{\partial [E_{ox}](x,t)}{\partial t} = D_E \frac{\partial^2 [E_{ox}](x,t)}{\partial x^2} + k_A [A][E_{red}] - \frac{k_{cat}[E_{ox}][S](x,t)}{K_M + [S](x,t)} \tag{9}$$

$$\frac{\partial [S](x,t)}{\partial t} = D_S \frac{\partial^2 [S](x,t)}{\partial x^2} - \frac{k_{cat}[E_{ox}][S](x,t)}{K_M + [S](x,t)} \tag{10}$$

This is a set of second order, partial, non-linear differential equations. We can simplify these by setting D_E to zero in Eq. (9), because the enzyme is immobilized within the hydrogel, and applying the steady state assumption to the enzyme ($\partial[E_{ox}](x,t)/\partial t = 0$). Then, in the steady state we are left with

$$D_A \frac{d^2[A]}{dx^2} = \frac{k_A k_{cat}[A][S][E_\Sigma]}{k_A[A](K_M + [S]) + k_{cat}[S]} \tag{11}$$

and

$$D_S \frac{d^2[S]}{dx^2} = \frac{k_A k_{cat}[A][S][E_\Sigma]}{k_A[A](K_M + [S]) + k_{cat}[S]} \tag{12}$$

where $[E_\Sigma] = [E_{ox}] + [E_{red}]$ is the total enzyme concentration in the film.

We now select an appropriate set of dimensionless variables. Thus, we normalise the concentrations of mediator and substrate and normalise the distance in the film by the film thickness

$$a = [A]/[A_\Sigma] \tag{13}$$

$$s = [S]/K_S[S]_\infty \tag{14}$$

$$\chi = x/l \tag{15}$$

where $[A_\Sigma]$ is the total concentration of mediator in the film, $[S_\infty]$ is the bulk concentration of substrate, and K_S is the partition coefficient of the substrate into the film (we assume partition is rapid). Lower case a and s are the dimensionless concentrations and χ is the dimensionless distance; all three lie between 0 and 1. We then select a further 4 dimensionless quantities that are characteristic ratios of the rate constants, concentrations and diffusion coefficients. This can be done in many different ways but we will always need 4 to describe the problem, and in choosing these we are guided by the chemistry of the problem. These four are

$$\kappa = l(\zeta k_A [E_\Sigma]/D_A)^{1/2} \tag{16}$$

$$\eta = (D_S \zeta k_A K_M)/(D_A k_{cat}) \tag{17}$$

$$\gamma = (k_A [A_\Sigma] K_M)/(k_{cat} K_S [S]_\infty) \tag{18}$$

$$\mu = K_S [S]_\infty / K_M \tag{19}$$

where κ describes the balance between the thickness of the hydrogel, l, and the reaction layer thickness for reduction of the oxidised mediator by the enzyme, $(D_A/k_A[E_\Sigma])^{1/2}$. η describes the balance between substrate reaction with the enzyme (k_{cat}/K_M) and mediator reaction with the enzyme (k_A) weighted by the relevant diffusion coefficients. γ describes the same ratio weighted by the relevant concentrations, and μ is the ratio of substrate in the film to the Michaelis constant so when μ is >1 the enzyme substrate kinetics are saturated.

Substituting in from Eqs. (13) to (19) in Eqs. (11) and (12) recasts the problem in dimensionless variables as [30]

$$\frac{d^2 a}{d\chi^2} = \frac{\kappa^2 a s}{\gamma a(1 + \mu s) + s} \tag{20}$$

and

$$\frac{d^2s}{d\chi^2} = \frac{\gamma\eta^{-1}\kappa^2 as}{\gamma a(1+\mu s)+s} \tag{21}$$

Clearly looking at Eqs. (20) and (21) we can see that we could equally well have chosen to replace η and/or κ by different dimensionless quantities

$$\xi_1 = \eta/\gamma = \left(D_S\zeta K_S[S]_\infty\right)/\left(D_A[A_\Sigma]\right) \tag{22}$$

and

$$\xi_2 = \kappa^2 = l^2\zeta k_A[E_\Sigma]/D_A \tag{23}$$

if we had wished, however the choice of κ makes more sense as it is proportional to the layer thickness. We now need to solve Eqs. (20) and (21) with the appropriate boundary conditions to obtain expressions of the current density, I. The current density is given by

$$I = \frac{nFD_A[A_\Sigma]J_{obs}}{l} \tag{24}$$

where J_{obs} is the dimensionless current. As we can see, for the steady state we need 4 dimensionless parameters to describe the steady state current density, I_{SS}, that is

$$I_{SS} = f(\kappa,\eta,\gamma,\mu) \tag{25}$$

Eqs. (20) and (21) do not have a simple analytical solution, therefore we derive a number of approximate analytical solutions corresponding to different limiting Cases [30] as shown schematically in Fig. 2. Cases I, II, IV and V as shown in Fig. 2 are straightforward (see for example Section 2.5 of [30] for the derivation of the Case I and II results). Cases III, VI and VII are more difficult and require some "tricks" to derive the approximate analytical expressions. For Case III (the titration case) the hydrogel is treated as two distinct regions, one near the electrode where the mediator is dominant, one near the outside where the substrate is dominant. The solution is then constructed by solving for the two regions separately and matching the conditions at the boundary within the film where they meet. Cases VI and VII are more complex and also require the film to be treated as two distinct regions. Full details of this and the treatment for all the Cases can be found in [30]. This analysis leads to the identification of seven separate Cases as defined in Table 1. Here by 'Case' we mean a physically distinct situation (e.g. Case I: current limited by the rate of reaction of the mediator with the enzyme when the reaction is occurring throughout the film) with a physical comprehensible solution (the current is given by the rate of the enzyme/mediator reaction multiplied by the film thickness).

6. The Case diagram

The Case diagram represents all possible behaviours for the model as described by the original equations and boundary conditions and shows graphically how the different Cases relate to each other. To understand the concept of the Case diagram it is useful to consider a simple, 1-dimensional example based on the familiar Michaelis Menten kinetics

$$\text{rate} = \frac{k_{cat}[E_\Sigma][S]}{[S]+K_M} \tag{26}$$

This has two limiting forms (Cases i and ii in Fig. 3). When $[S] << K_M$ the kinetics are unsaturated and the rate increases linearly with [S]

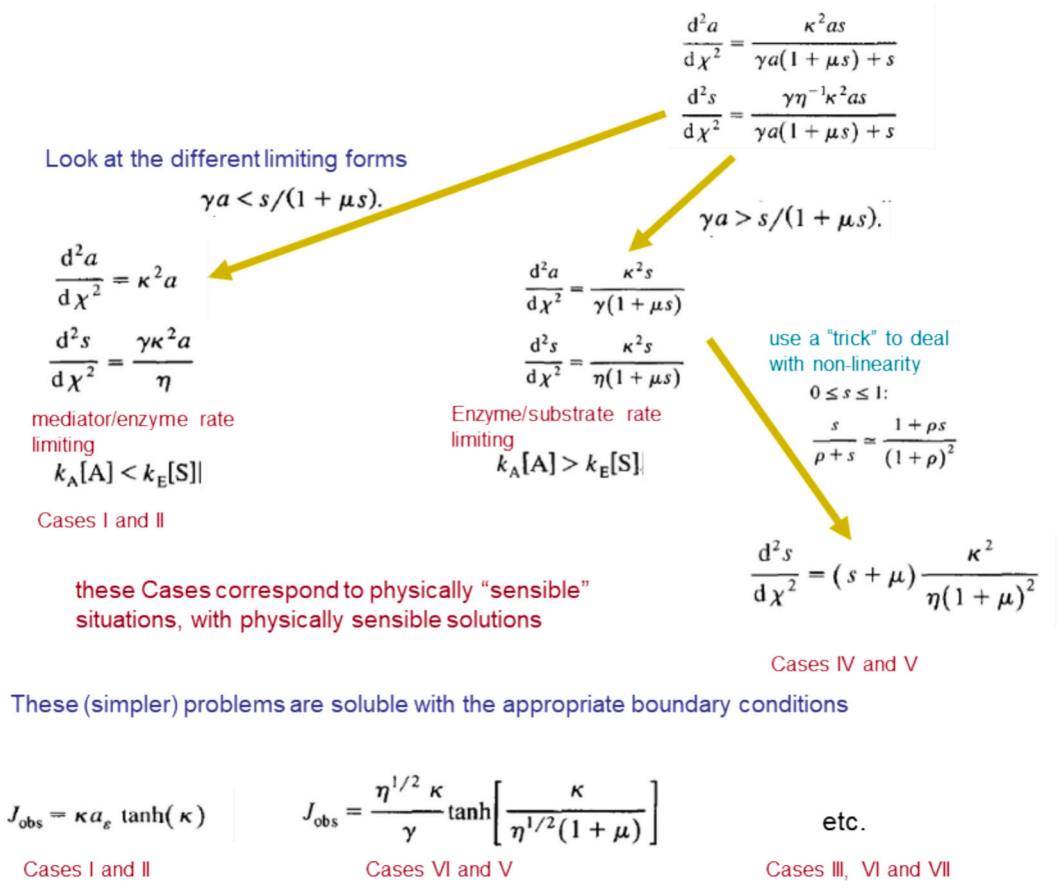

Fig. 2. Schematic of the method for deriving the different approximate analytical solutions. (Here $k_E = k_{cat}/(K_M + [S])$ is the effective rate constant for reaction of the enzyme with the substrate.) Full details of the derivation can be found in [30].

Table 1
Expressions for the current density in the different Cases. (From [30,31] assuming $a_\varepsilon = 1$, corresponding to the limiting current for reoxidation of the mediator at the electrode. $a_\varepsilon = (1 + \exp(-\varepsilon))^{-1}$ where $\varepsilon = (E - E^0)nF/RT$ is the dimensionless potential. The expressions for Cases III and VI have been corrected for a typographical error in [31].)

Case	Kinetics limited by:	Approximate dimensionless current, J_{obs}	Approximate analytical expression for the steady state current density, I_{ss}
I	enzyme-mediator reaction, thin film	κ^2	$\zeta nF[A_\Sigma]k_A[E_\Sigma]l$
II	enzyme-mediator reaction, thick film	κ	$nF[A_\Sigma]\sqrt{\zeta D_A k_A[E_\Sigma]}$
III	titration case	$1+\eta/\gamma$	$nF(D_A[A_\Sigma]+\zeta D_S K_S[S]_\infty)/l$
IV	substrate-enzyme reaction, thick film	$\dfrac{\eta^{1/2}\kappa}{\gamma\left(1+\frac{1}{2}\mu\right)^{1/2}}$	$\zeta nFK_S[S]_\infty\sqrt{k_{cat}[E_\Sigma]D_S/\left(K_M+\frac{1}{2}K_S[S]_\infty\right)}$
V	substrate-enzyme reaction, thin film	$\dfrac{\kappa^2}{\gamma(1+\mu)}$	$\zeta nF\{l[E_\Sigma]k_{cat}K_S[S]_\infty/(K_M+K_S[S]_\infty)\}$
VI	transition Case, substrate totally depleted	$(2\kappa^2\eta/\gamma)^{1/2}$	$nF\zeta\sqrt{2[A_\Sigma]k_A[E_\Sigma]D_S K_S[S]_\infty}$
VII	transition Case, mediator totally depleted	$\{2\kappa^2/\gamma(1+\mu)\}^{1/2}$	$nF\sqrt{2\zeta D_A[A_\Sigma]k_{cat}[E_\Sigma]K_S[S]_\infty/(K_M+K_S[S]_\infty)}$

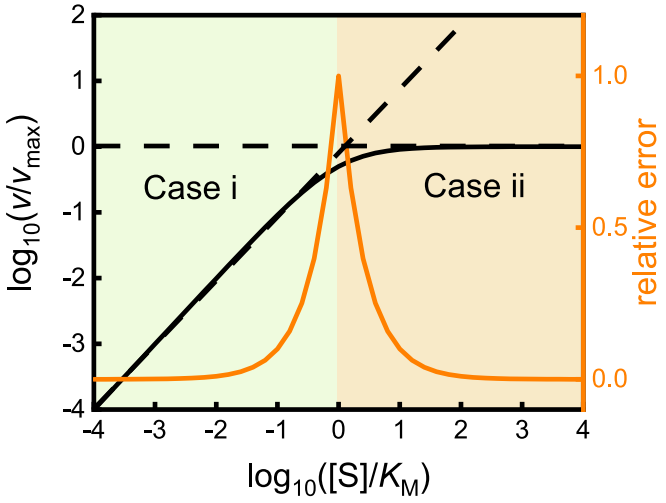

Fig. 3. One-dimensional Case diagram for Michaelis Menten kinetics showing the two limiting cases (dashed lines), the full solution (solid black line), and the relative error in the approximate solutions (orange).

$$\text{rate}_i \approx \frac{k_{cat}[E_\Sigma][S]}{K_M} \tag{27}$$

When $[S] >> K_M$ the kinetics are saturated and the rate is independent of [S]

$$\text{rate}_{ii} \approx k_{cat}[E_\Sigma] \tag{28}$$

The boundary between the two Cases occurs when $[S] = K_M$. Notice that on the Case boundary the two approximate expressions for the rate in Eqs. (27) and (28) are equal and that this value ($k_{cat}[E_\Sigma]$) is twice the actual value ($k_{cat}[E_\Sigma]/2$) given by Eq. (26).

The corresponding Case diagram is shown in Fig. 3 where the *x*-axis is the log of the dimensionless parameter, $[S]/K_M$, that describes this system and the rate is plotted on the *y* axis. Notice that on the boundary of the two cases the two approximate expressions for the rate, Eqs. (27) and (28) give the same result. The approximate solutions become very good approximations to the full result given by Eq. (26) as we move away from the boundary, and the error (in this case a factor of 2) is greatest on the Case boundary.

The Case diagram is closely related to the zone diagrams used by Savéant and colleagues [32–36] which also summarise the different kinetic behaviours of the system and their interrelation. A key difference is that Savéant introduces additional transitional zones that replace the Case boundaries.

For the redox-hydrogel enzyme electrode model discussed here the current depends on the four dimensionless parameters, κ, η, γ, and μ. Consequently the full parameter space for this problem is 4-dimensional. While a Case diagram can help to visualize the relationship between the different kinetic regimes in the parameter space it is necessary to simplify its representation since we cannot readily represent the 4-dimensional Case diagram on the page. Simpler versions of the Case diagram can be generated by fixing the values of one or two of the dimensionless parameters in order to reduce the diagram to a 3 or 2-dimensional plot such as those shown in Figs. 4 and 5. The 3-dimensional Case diagram in Fig. 4 is drawn for $\mu < 1$, the 2-dimensional Case diagram in Fig. 5 is drawn for $\eta = 1$ and $\mu < 1$. Thus, both correspond to unsaturated enzyme substrate kinetics with $K_S[S]_\infty/K_M < 1$.

The location of the boundaries between Cases is determined by the approximations that split the full problem into the different soluble approximate analytical solutions. For example, when $\gamma a < s/(1+\mu s)$, corresponding to $k_A[A] < k_{cat}[S]/(K_M + [S])$ (see Fig. 2), Eqs. (20) and (21) simplify to

$$\frac{d^2a}{d\chi^2} = \kappa^2 a \tag{29}$$

and

$$\frac{d^2s}{d\chi^2} = \gamma\eta^{-1}\kappa^2 a \tag{30}$$

which can be solved with the appropriate boundary conditions to give, for the dimensionless current density, J_{obs},

$$J_{obs} = \kappa\, tanh(\kappa) \tag{31}$$

This has two limiting forms. For small κ, $J_{obs} \approx \kappa^2$, and for large κ, $J_{obs} \approx \kappa$. These correspond to the solutions for Cases I and II (see Table 1) and the boundary between them occurs for $\kappa = 1$ corresponding to $\log\kappa = 0$ in Figs. 4 and 5. Note also that the requirement that $\gamma a < s/(1+\mu s)$ restricts the two cases to the region where $\gamma < 1$ in Figs. 4 and 5. The other boundaries between Cases are derived by similar logic. Note that on the boundary the two limiting expressions for J_{obs}, in this case κ and κ^2, are equal, but are larger than the value given by Eq. (31) of 0.762. As for the simple Michaelis Menten example discussed above and illustrated in Fig. 3, the approximate analytical solutions are least accurate at the Case boundaries. To obtain accurate values in the boundary regions we need to turn to numerical modelling. The combination of the approximate analytical solutions and the numerical modelling then gives a full description of the system [30]. This approach has been extended by Fourmond and Léger and by Li et al. to characterise the penetration of oxygen into oxygen-sensitive enzyme redox polymer films [37,38].

Various examples of the application of the approximate analytical approach, with the corresponding Case diagrams, to a variety of electrochemical and related problems can be found in the literature and some examples are summarised in Table 2.

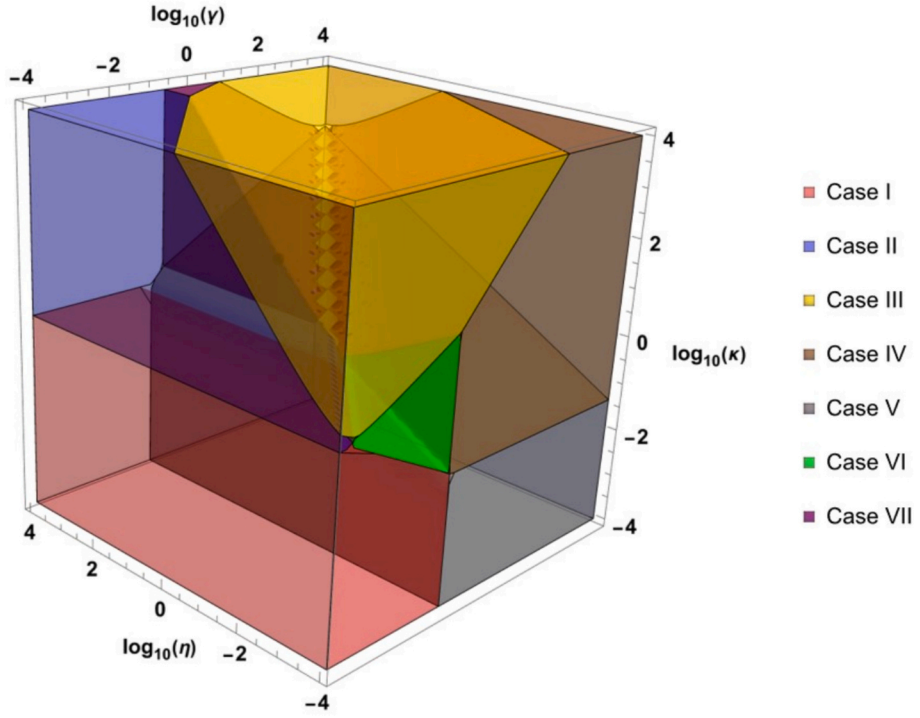

Fig. 4. Three-dimensional representation of the Case diagram drawn for $\mu < 1$. The figure was created in Mathematica® using the 'RegionPlot3D' command/function and the expressions for the Case boundaries given in Table 2 of reference [30].

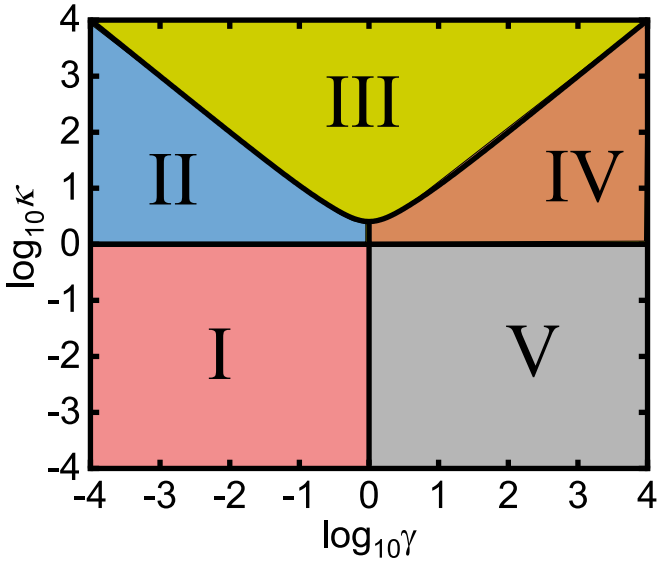

Fig. 5. Two-dimensional Case diagram plotted for $\eta = 1$ and $\mu < 1$ (adapted from [30]). Increasing film thickness, l, moves you vertically on the diagram, increasing bulk substrate concentration, $[S]_\infty$, moves you to the left.

7. How to use the Case diagram

The important thing about the Case diagram is that it encompasses **all** of the possible behaviours of the model described by the original equations and boundary conditions and provides a 'map' of the mathematical terrain. By this we mean that if you know where you are in the Case diagram then you know how to navigate to any other location in the Case diagram by changing experimental variables. Thus, for example if you know that we are in Case I in Fig. 5 then you know we can move to Case II by increasing the film thickness, l, since this will increase κ.

Table 2
Examples of Case diagrams in the literature.

Electrochemical system	Reference
Photoelectrochemistry at the optically transparent rotating disc electrode	Albery et al. [39–41]
Photogalvanic cells	Albery and Archer [18,19]
Redox catalysis at a modified electrode	Albery and Hillman [7]
Semiconductor photoelectrochemistry	Albery et al. [42,43]
Microheterogeneous electrodes	Albery and Bartlett [44]
Colloidal semiconductor photoelectrochemistry	Albery and Bartlett [45]
Heterogeneous mediated enzyme electrode	Albery et al. [46]
Second order ECE reaction at RDE	Bartlett and Eastwick-Field [47]
Enzyme immobilized in electropolymerized film	Bartlett and Whitaker [48]
Homogeneous enzyme mediation at RDE	Bartlett and Pratt [49]
Multi-component modified electrode	Lyons et al. [50]
Diffusion and binding in a film	Bartlett and Gardner [20]
Redox catalysis at polymer modified microelectrode	Rebouillat et al. [51,52]
Redox active monolayer electrode	Lyons [53,54]
Enzyme immobilized in electronically conducting film	Lyons [55,56]
Enzyme electrode in the thin layer limit	Lyons [57]
Electroactive-enzyme electrode	Lyons [58]
Microheterogeneous thin film electrode	Lyons [59]

Equally if you want to move from Case I to Case V then you can do this by decreasing the substrate concentration, $[S]_\infty$, since this will increase γ.

To illustrate how the Case diagram is related to the experiment let us consider data for an osmium polyelectrolyte mediated glucose electrode fabricated by layer-by-layer self-assembly [31]. The self-assembly technique [60], in which the electrode is sequentially dipped in solutions of the polycationic osmium redox polymer and the polyanionic enzyme, allows fine control over the film thickness. In the experiments measurements were carried out for 7 different electrodes with film thicknesses between 87 and 1150 nm for glucose concentrations from

0 to 55 mM. Experimentally varying film thickness and glucose concentration means varying κ and μ while keeping η and $\gamma\mu$ constant. Fig. 6 shows a projection of the Case boundaries, calculated using the equations given in Table 2 of [30], onto the logμ, logκ plane calculated for η = 400 and $\gamma\mu$ = 0.519. Increasing $[S]_\infty$ in the logκ, logη, logγ, logμ 4-dimensional Case diagram corresponds to moving in both the logμ and -logγ directions. Making the plot with $\gamma\mu$ held constant is one way to overcome this. Another way would be to plot the Case diagram in the logη, log$(\mu/\gamma)^{1/2}$ plane. The values of η and $\gamma\mu$ used to make Fig. 6 have been calculated based on best estimates of diffusion coefficients and rate constants from other measurements [31]. The shaded region in the figure corresponds to the region of the logμ, logκ plane explored in this set of experiments. The signposts in the corner of the figure indicate the direction of movement on increasing film thickness, l, or bulk glucose concentration, $[S]_\infty$. From the figure we can see that the experiments potentially lie in Cases I, II, V or VII.

Plotting the experimental data against the osmium surface loading (which is proportional to film thickness) for saturating concentrations of glucose, Fig. 7a, shows that the results fit to Cases I and II, shifting from Case I to Case II as the thickness, and thus κ, increases. This corresponds to moving vertically in the logμ, logκ plane in Fig. 6. The solid line in Fig. 7a corresponds to the fit of the data to Eq. (30). At the Case boundary, as expected, the deviation between the experimental data and the approximate analytical solutions for Cases I and II is at its largest. Note that the scatter in the data in Fig. 7a reflects the variation from electrode to electrode. Achieving good reproducibility in electrode fabrication is one of the challenges of fitting experimental data to the model.

At lower, non-saturating, glucose concentrations the system lies in Cases V and VII, with the thin films (smaller κ) being in Case V. Fig. 7b shows the data for thinner films plotted against glucose concentration (see Table 1) for Case V and Fig. 7c shows the data for thicker films plotted against the square root of glucose concentration for Case VII (see Table 1). The results show the predicted change in dependence of glucose concentration as the film thickness increases.

8. Does the model fit your data?

When starting out trying to fit experimental data to the model the problem is to find out whereabouts in the 4-dimensional space you are. Any single calibration plot can only give limited information, essentially

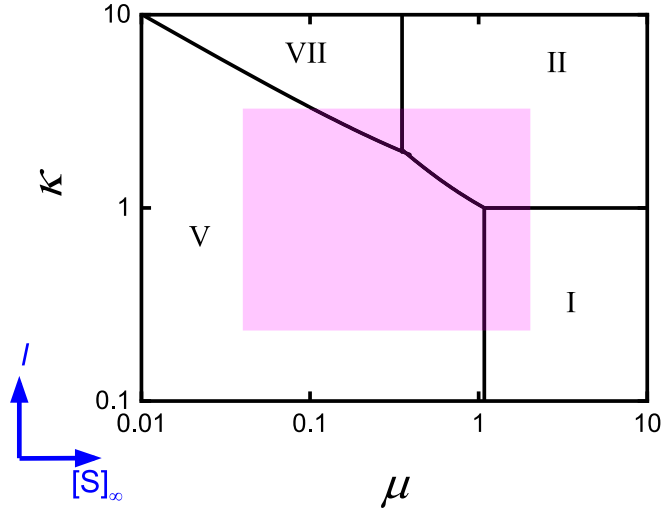

Fig. 6. Case diagram for the β-D-glucose/GOx/PAH-Os system (adapted from [31]). The diagram is the projection onto the logκ, logμ plane for constant values of η and $\gamma\mu$ (400 and 0.519 respectively). Increasing bulk glucose concentration corresponds to moving along the x-axis and increasing film thickness corresponds to moving along the y-axis.

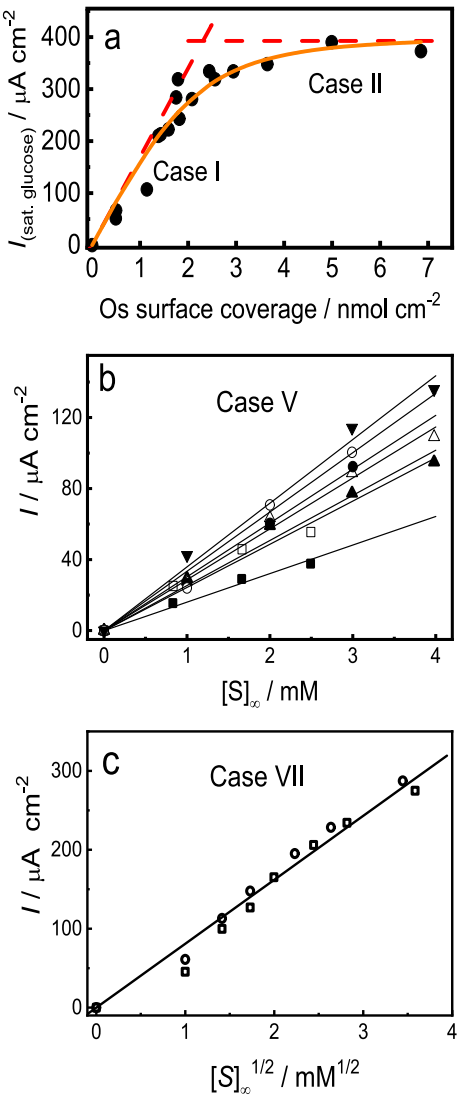

Fig. 7. Analysis of results for the β-D-glucose/GOx/PAH-Os system (adapted from [31]). a) Catalytic current at glucose saturation as a function of the osmium loading (proportional to film thickness). The dashed lines are the Case I and Case II expressions, the orange line is the best fit to Eq. (30). b) Plot of the catalytic current against the glucose concentration for 7 different film thicknesses from 87 to 430 nm. The lines are the best fits to the data for Case V. c) Plot of the catalytic current against the square root of the glucose concentration for film thicknesses of □ 0.613 and ○ 1.15 μm. The line is the best fit to Case VII.

the initial slope and the response at saturating substrate concentration, and this is not enough to fix the position. Thus, a set of experiments for different conditions is required together with independent values for as many of the experimental variables as possible for other experiments. For example, an independent measurement of D_A from a chronoamperometric experiment or a measurement of I from ellipsometry. Good examples of this can be found in the literature [31,61–63]. For the model here we know that the response is a function of the four dimensionless parameters, $I_{ss} = f(\kappa,\eta,\gamma,\mu)$. However, the values of these four parameters depend on 11 experimental variables: the electrode potential (E), $[S]_\infty$, l, $[E_\Sigma]$, $[A_\Sigma]$, k_A, D_A, D_S, K_S, k_{cat}, and K_M. Some of these experimental variables, E and $[S]_\infty$, are easy to change, others, l, $[E_\Sigma]$ and $[A_\Sigma]$, are more difficult to alter and require experiments with multiple electrodes so that reproducibility in electrode fabrication is essential. Finally, some, k_A, D_A, D_S, K_S, k_{cat}, and K_M, are more difficult still and require changes in the chemistry of the system. There are some approaches that can be useful such as changing the substrate as a way to

change the enzyme-substrate kinetics. For example, using 2-deoxy-D-glucose instead of D-glucose for experiments with glucose oxidase [64], or mixing active and inactive enzyme as a way to alter [E_Σ] without changing the physical properties of the layer. It is also important to vary the external mass transport, possibly using a rotating disc electrode, to confirm that external mass transport is not a significant factor, or if it is to correct for it [65–67].

In the context of locating the experimental system in the Case diagram it is useful to consider the functional dependence of the current in the different Cases on the experimental variables, Table 3. For example, if the current increases linearly with increasing substrate concentration the system must be in Case III, IV or V. Changing the enzyme loading or layer thickness then allows the three possibilities to be distinguished since for Case III the current is independent of enzyme loading but decreases as thickness increases, for Case IV the current varies with the square root of enzyme loading and is independent of thickness, and for Case V the current increases linearly with enzyme loading and increases linearly with thickness. Inspection of Table 3 shows that only Cases VI and VII share the same 'fingerprint'. When using this approach one should be aware that you might cross a Case boundary as the experimental conditions change, for example see Fig. 7a where Case I turns into Case II as the thickness increases.

Once we have worked out where we are in the Case diagram we can fit the experimental results to the numerical model since we know the approximately correct values for the dimensionless parameters [31,68]. We can then use numerical simulation guided by the Case diagram to explore the boundaries between Cases and/or the transient behaviour using bespoke programs created in commercial software such as MATLAB®, Mathematica®, or COMSOL Multiphysics®.

Looking forward we would like to draw attention to an exciting innovation by Plumére and Johnson [69] who have developed a computational method that maps the entire parameter space for a multidimensional electrochemical system and then automatically identifies kinetic regimes. In this approach the model is nondimensionalised and implemented numerically in suitable software (e.g. MATLAB® or COMSOL Multiphysics®) to generate the dimensionless current function. The current output over a discrete set of parameters is interpreted as a parametrized geometric surface and the Zone boundaries and limiting Zones are defined by the curved and flat regions, respectively. This definition of a limiting Zone corresponds to a region where the dimensionless current has a power law dependence on the dimensionless parameters. In terms of Eq. (25) and the model we have discussed here this means that

$$I_{\text{limiting Zone}} \propto \kappa^{a} \eta^{b} \gamma^{c} \mu^{d} \tag{32}$$

where a, b, c and d are all constants. This is not the same as the definition of the Cases used here and in [30,31]. For example, inspection of Table 1 shows that Cases I, II and VI obey Eq. (32) and therefore are limiting Zones according to Plumére and Johnson but Cases III, IV, V and VI would each be split into two limiting Zones giving a total of 11 limiting Zones corresponding to the 7 Cases. The redox-hydrogel enzyme electrode model discussed here is one of the examples treated in depth as an exemplar of the new approach and further details can be found in Plumére and Johnson's paper [69]. This new computational approach is exciting because it utilises the enormous computational capability now available and can be applied to electrochemical systems with intrinsically high complexity. The challenge will be to put a physico-chemical interpretation onto the limiting Zones.

Table 3
The dependence of the enzyme electrode current on the different experimental variables.

Case	[S]	[A]	[Ez]	l (thickness)
I	0	1	1	1
II	0	1	½	0
III $\eta/\gamma < 1$	1	0	0	-1
$\eta/\gamma > 1$	0	0	0	-1
IV $\mu < 2$	1	0	½	0
$\mu > 2$	½	0	½	0
V $\mu < 1$	1	0	1	1
$\mu > 1$	0	0	1	1
VI	1/2	1/2	1/2	0
VII $\mu < 1$	1/2	1/2	1/2	0
$\mu > 1$	0	1/2	1/2	0

9. Why is modelling and the Case diagram useful?

The most important benefit that we get from the approximate analytical analysis and the Case diagram is insight into the different factors that affect the enzyme electrode output and the direct interplay between them. We can then use this insight to identify the important factors and to look for effects that we have not included in the model, such as product inhibition. We can also use the model to predict the response and to improve the electrode design. The Case diagram allows us to identify the optimum values for our dimensional parameters for a particular application. If we know where we are in the Case diagram, we can also identify which experimental variables, for example enzyme loading, film thickness or degree of hydrogel crosslinking, to change in order to move to a different Case.

In terms of designing a practical amperometric enzyme electrode there are a number of design factors that need to be considered. These include the response time (i.e. the time taken to achieve a fraction, typically 90 %, of the full response), the sensitivity and range (how the response changes with increasing substrate concentration). In terms of commercial manufacture, the manufacturing tolerances (which variables have the greatest effect on sensor response and how these can be controlled during manufacture, and what level of tolerance is required) are an important consideration. For example, in Case III the response does not depend on enzyme kinetics which means if one batch of enzyme varies in activity from another it should not have an effect on the sensor response within reason. Stability in storage and in use are also important design factors. Similar considerations apply for other applications of enzyme electrodes such as for biofuel cells and for bioelectrosynthesis.

10. Conclusions

Notwithstanding the enormous advances in computing power and availability of powerful commercial modelling software approximate analytical approaches remain an important tool in modelling complex coupled diffusion/reaction problems because of the insight that they provide into the underlying physical chemistry. The approximate analytical models allow us to construct Case diagrams that encompass all of the different possible behaviours and demonstrate the relationships between them. In this way the Case diagram maps out the terrain and encapsulates the insights gained from the approximate analytical treatment of the problem. The most powerful approach to modelling coupled diffusion/reaction problems is, then, to combine the approximate analytical treatment with accurate numerical solution using the numerical solution to explore the transient behaviour and to provide greater accuracy in the regions of the Case boundaries.

In the case of the amperometric enzyme electrode, matching experimental data to the model is challenging because of the large number of experimental variables involved and their interdependences. Thus, it requires multiple measurements with multiple electrodes, and this demands high reproducibility and control over electrode fabrication. In essence it requires the ability to prepare sensors whose response can be accurately predicted so that they do not require calibration. However, once the location within the Case diagram is established this modelling and insight from the Case diagram allows rational design and optimisation of the sensor performance since it tells us which way to move within the solution space and what is possible.

CRediT authorship contribution statement

Philip N. Bartlett: Writing – review & editing, Writing – original draft, Supervision, Project administration, Methodology, Funding acquisition, Conceptualization. **M. Hashim Khan:** Writing – review & editing, Software, Methodology, Conceptualization.

Declaration of competing interest

The authors declare that they have no known competing financial interests or personal relationships that could have appeared to influence the work reported in this paper.

Acknowledgements

This publication is part of a project that received funding from the European Union's Horizon 2020 research and innovation program under grant agreement No. 813006 (Marie Skłodowska-Curie MSCA-ITN "ImplantSens").

Data availability

Data will be made available on request.

References

[1] A. Heller, Electrical wiring of redox enzymes, Acc. Chem. Res. 23 (1990) 128–134.
[2] S. Feldberg, Auerbach, model for current reversal chronopotentiometry with second-order kinetic complications, Anal. Chem. 36 (1964) 505.
[3] T. Joslin, D. Pletcher, Digital-simulation of electrode processes - procedures for conserving computer time, J. Electroanal. Chem. 49 (1974) 171–186.
[4] D. Britz, Digital Simulation in Electrochemistry, Springer-Verlag, Berlin Heidelberg, 1981.
[5] D. Britz, J. Strutwolf, Digital Simulation in Electrochemistry, in: 4th Edition Digital Simulation in Electrochemistry, 4th edition, 2016, pp. 1–492.
[6] C. Andrieux, J.M. Dumas-Bouchiat, J.M. Saveant, Catalysis of electrochemical reactions at redox polymer electrodes - kinetic-model for stationary voltammetric techniques, J. Electroanal. Chem. 131 (1982) 1–35.
[7] W.J. Albery, A.R. Hillman, Transport and kinetics in modified electrodes, J. Electroanal. Chem. 170 (1984) 27–49.
[8] E.J. Calvo, C. Danilowicz, L. Diaz, Enzyme catalysis at hydrogel-modified electrodes with redox polymer mediator, J. Chem. Soc. Faraday Trans. 89 (1993) 377–384.
[9] T. Tatsuma, T. Watanabe, Theoretical evaluation of mediation efficiency in enzyme-incorporated electrodes, Anal. Chem. 65 (1993) 3129–3133.
[10] M. Marchesiello, E. Genies, A theoretical-model for an amperometric glucose sensor using polypyrrole as the immobilization matrix, J. Electroanal. Chem. 358 (1993) 35–48.
[11] C. Bourdillon, C. Demaille, J. Moiroux, J.M. Saveant, Catalysis and mass-transport in spatially ordered enzyme assemblies on electrodes, J. Am. Chem. Soc. 117 (1995) 11499–11506.
[12] P.N. Bartlett, C.S. Toh, E.J. Calvo, V. Flexer, Modelling biosensor responses, in: P. N. Bartlett (Ed.), Bioelectrochemistry. Fundamentals, Experimental Techniques and Applications, Wiley, 2008.
[14] A.R. Jalalvand, M. Roushani, H.C. Goicoechea, D.N. Rutledge, H.W. Gu, MATLAB in electrochemistry: a review, Talanta 194 (2019) 205–225.
[15] E.J.F. Dickinson, H. Ekström, E. Fontes, COMSOL Multiphysics®: finite element software for electrochemical analysis. A mini-review, Electrochem. Commun. 40 (2014) 71–74.
[16] A. Heller, B. Feldman, Electrochemistry in diabetes management, Acc. Chem. Res. 43 (2010) 963–973.
[17] A. Heller, Electron-conducting redox hydrogels: design, characteristics and synthesis, Curr. Opin. Chem. Biol. 10 (2006) 664–672.
[18] W.J. Albery, M.D. Archer, Photogalvanic cells. 3. Maximum power obtainable from a thin-layer photogalvanic concentration cell with identical electrodes, J. Electroanal. Chem. 86 (1978) 1–18.
[19] W.J. Albery, M.D. Archer, Photogalvanic cells. 4. Maximum power from a thin-layer cell with differential electrode-kinetics, J. Electroanal. Chem. 86 (1978) 19–34.
[20] P.N. Bartlett, J.W. Gardner, Diffusion and binding of molecules to sites within homogeneous thin films, Philosophical Trans. Royal Soc. A-Math. Phys. Eng. Sci. 354 (1996) 35–57.
[21] H. Dahms, Electronic conduction in aqueous solution, J. Phys. Chem. 72 (1968) 362–364.
[22] I. Ruff, L. Botar, Effect of exchange-reactions on transport processes - a comparison of thermodynamic treatment with random-walk on lattice points, J. Chem. Phys. 83 (1985) 1292–1297.
[23] I. Ruff, V.J. Fredrich, Transfer diffusion. I. Theoretical, J. Phys. Chem. 75 (1971) 3297–3302.
[24] M.E.G. Lyons, Charge Percolation in Electroactive Polymers, Plenum Press, New York, In Electroactive Polymer Electrochemistry, 1994.
[25] D.N. Blauch, J.M. Saveant, Dynamics of electron hopping in assemblies of redox centers - percolation and diffusion, J. Am. Chem. Soc. 114 (1992) 3323–3332.
[26] A. Aoki, A. Heller, Electron-diffusion coefficients in hydrogels formed of cross-linked redox polymers, J. Phys. Chem. 97 (1993) 11014–11019.
[27] R. Wilson, A.P.F. Turner, Glucose-oxidase - an ideal enzyme, Biosens. Bioelectron. 7 (1992) 165–185.
[28] C. Bourdillon, C. Demaille, J. Moiroux, J.M. Saveant, From homogeneous electroenzymatic kinetics to antigen-antibody construction and characterization of spatially ordered catalytic enzyme assemblies on electrodes, Acc. Chem. Res. 29 (1996) 529–535.
[29] V. Flexer, M.V. Ielmini, E.J. Calvo, P.N. Bartlett, Extracting kinetic parameters for homogeneous $Os(bpy)_2ClPyCOOH^+$ mediated enzyme reactions from cyclic voltammetry and simulations, Bioelectrochemistry 74 (2008) 201–209.
[30] P.N. Bartlett, K.F.E. Pratt, Theoretical treatment of diffusion and kinetics in amperometric immobilized enzyme electrodes. 1. Redox mediator entrapped within the film, J. Electroanal. Chem. 397 (1995) 61–78.
[31] V. Flexer, E.J. Calvo, P.N. Bartlett, The application of the relaxation and simplex method to the analysis of data for glucose electrodes based on glucose oxidase immobilised in an osmium redox polymer, J. Electroanal. Chem. 646 (2010) 24–32.
[32] C. Costentin, B. Limoges, M. Robert, C. Tard, A pioneering career in electrochemistry: Jean-Michel Saveant, ACS Catal. 11 (2021) 3224–3238.
[33] J.M. Savéant, Molecular catalysis of electrochemical reactions.: mechanistic aspects, Chem. Rev. 108 (2008) 2348–2378.
[34] C. Costentin, J.M. Savéant, Cyclic voltammetry of Electrocatalytic films: fast catalysis regimes, ChemElectroChem 2 (2015) 1774–1784.
[35] B. Johnson, A.M. Beiler, B.D. McCarthy, S. Ott, Transport phenomena: challenges and opportunities for molecular catalysis in metal-organic frameworks, J. Am. Chem. Soc. 142 (2020) 11941–11956.
[36] B. Johnson, S. Ott, Diagnosing surface *versus* bulk reactivity for molecular catalysis within metal-organic frameworks using a quantitative kinetic model, Chem. Sci. 11 (2020) 7468–7478.
[37] V. Fourmond, C. Léger, Theoretical understanding of the penetration of O_2 in enzymatic redox polymer films: the case of unidirectional catalysis and irreversible inactivation in a film of arbitrary thickness, ChemElectroChem 8 (2021) 2607–2615.
[38] H.G. Li, D. Buesen, S. Dementin, C. Léger, V. Fourmond, N. Plumeré, Complete protection of O_2-sensitive catalysts in thin films, J. Am. Chem. Soc. 141 (2019) 16734–16742.
[39] C. Boxall, W.J. Albery, Photoelectrochemistry with the optical rotating disc electrode - part 3. The theoretical analysis for photophysical-chemical-electrochemical (PCE) processes, Phys. Chem. Chem. Phys. 2 (2000) 3651–3662.
[40] C. Boxall, W.J. Albery, Photoelectrochemistry with the optical rotating disc electrode - part 1. The theoretical analysis for photophysical-electrochemical processes, Phys. Chem. Chem. Phys. 2 (2000) 3631–3639.
[41] W.J. Albery, W.R. Bowen, F.S. Fisher, A.D. Turner, Photogalvanic cells. 8. Theory of the transparent rotating-disk electrode, J. Electroanal. Chem. 107 (1980) 1–9.
[42] W.J. Albery, P.N. Bartlett, The recombination of photogenerated minority-carriers in the depletion layer of semiconductor electrodes, J. Electrochem. Soc. 130 (1983) 1699–1706.
[43] W.J. Albery, P.N. Bartlett, A. Hamnett, M.P. Dare-Edwards, The transport and kinetics of minority-carriers in illuminated semiconductor electrodes, J. Electrochem. Soc. 128 (1981) 1492–1501.
[44] W.J. Albery, P.N. Bartlett, Transport and kinetics at microheterogeneous electrodes. 1. The collection efficiency, J. Electroanal. Chem. 131 (1982) 137–144.
[45] W.J. Albery, P.N. Bartlett, The transport and kinetics of photogenerated carriers in colloidal semiconductor electrode particles, J. Electrochem. Soc. 131 (1984) 315–325.
[46] W.J. Albery, P.N. Bartlett, B.J. Driscoll, R.B. Lennox, Amperometric enzyme electrodes. 5. The homogeneous mediated mechanism, J. Electroanal. Chem. 323 (1992) 77–102.
[47] P.N. Bartlett, V. Eastwick-Field, Theoretical-analysis for a 2nd-order ECE process at a rotating-disk electrode, journal of the chemical society-faraday, Transactions 89 (1993) 213–218.
[48] P.N. Bartlett, R.G. Whitaker, Electrochemical immobilization of enzymes. 1. Theory, J. Electroanal. Chem. 224 (1987) 27–35.
[49] P.N. Bartlett, K.F.E. Pratt, A study of the kinetics of the reaction between ferrocene monocarboxylic acid and glucose-oxidase using the rotating-disc electrode, J. Electroanal. Chem. 397 (1995) 53–60.
[50] M.E.G. Lyons, D.E. McCormack, O. Smyth, P.N. Bartlett, Transport and kinetics in multicomponent chemically modified electrodes, Faraday Discuss. 88 (1989) 139–149.
[51] S. Rebouillat, M.E.G. Lyons, A. Flynn, Heterogeneous redox catalysis at conducting polymer ultramicroelectrodes, Analyst 124 (1999) 1635–1644.
[52] S. Rebouillat, M.E.G. Lyons, A. Flynn, Mediated electron transfer at conducting polymer ultramicroelectrodes, Analyst 125 (2000) 1611–1628.
[53] M.E.G. Lyons, Mediated electron transfer at redox active monolayers. Part 3: bimolecular outer-sphere, first order Koutecky-Levich and adduct formation mechanisms, Sensors 2 (2002) 473–506.
[54] M.E.G. Lyons, The mechanism of mediated electron transfer at redox active surfaces, Electroanalysis 27 (2015) 992–1009.

[55] M.E.G. Lyons, Transport and kinetics in electrocatalytic thin film biosensors: bounded diffusion with non-Michaelis-Menten reaction kinetics, J. Solid State Electrochem. 24 (2020) 2751–2761.
[56] M.E.G. Lyons, Transport and kinetics in electrocatalytic thin film conducting polymer biosensors: bounded diffusion with Michaelis-Menten kinetics incorporating general inhibition effects, Int. J. Electrochem. Sci. 15 (2020) 6060–6090.
[57] M.E.G. Lyons, Mediated electron transfer at redox active monolayers. Part 4: kinetics of redox enzymes coupled with electron mediators, Sensors 3 (2003) 19–42.
[58] M.E.G. Lyons, Modelling the transport and kinetics of electroenzymes at the electrode/solution interface, Sensors 6 (2006) 1765–1790.
[59] M.E.G. Lyons, Understanding the kinetics of catalysed reactions in microheterogeneous thin film electrodes, J. Electroanal. Chem. 872 (2020) 114278.
[60] J. Hodak, R. Etchenique, E.J. Calvo, K. Singhal, P.N. Bartlett, Layer-by-layer self-assembly of glucose oxidase with a poly(allylamine)ferrocene redox mediator, Langmuir 13 (1997) 2708–2716.
[61] J.W. Gallaway, S.A.C. Barton, Kinetics of redox polymer-mediated enzyme electrodes, J. Am. Chem. Soc. 130 (2008) 8527–8536.
[62] H.M. Bambhania, D. Chakraborty, H. Wen, S.C. Barton, Impact of oxygen on glucose oxidation kinetics in a redox polymer mediated glucose oxidase electrode, J. Electrochem. Soc. 164 (2017) H232–H240.
[63] V. Fourmond, S. Stapf, H.G. Li, D. Buesen, J. Birrell, O. Rüdiger, W. Lubitz, W. Schuhmann, N. Plumeré, C. Léger, Mechanism of protection of catalysts supported in redox hydrogel films, J. Am. Chem. Soc. 137 (2015) 5494–5505.
[64] M.R. Sierks, K. Bock, S. Refn, B. Svensson, Active-site similarities of glucose-dehydrogenase, glucose-oxidase, and glucoamylase probed by deoxygenated substrates, Biochemistry 31 (1992) 8972–8977.
[65] P.N. Bartlett, P.R. Birkin, E.N.K. Wallace, Oxidation of beta-nicotinamide adenine dinucleotide (NADH) at poly(aniline)-coated electrodes, journal of the chemical society-faraday, Transactions 93 (1997) 1951–1960.
[66] P.N. Bartlett, E.N.K. Wallace, The oxidation of β-nicotinamide adenine dinucleotide (NADH) at poly(aniline)-coated electrodes part II.: kinetics of reaction at poly (aniline)- poly(styrenesulfonate) composites, J. Electroanal. Chem. 486 (2000) 23–31.
[67] P.N. Bartlett, E.N.K. Wallace, The oxidation of ascorbate at poly(aniline)-poly (vinylsulfonate) composite coated electrodes, Phys. Chem. Chem. Phys. 3 (2001) 1491–1496.
[68] V. Flexer, K.F.E. Pratt, F. Garay, P.N. Bartlett, E.J. Calvo, Relaxation and simplex mathematical algorithms applied to the study of steady-state electrochemical responses of immobilized enzyme biosensors: comparison with experiments, J. Electroanal. Chem. 616 (2008) 87–98.
[69] N. Plumeré, B. Johnson, A geometric interpretation of kinetic zone diagrams in electrochemistry, J. Am. Chem. Soc. 146 (2024) 34771–34785.